2013 European Control Conference (ECC)
July 17-19, 2013, Zürich, Switzerland.

The Cubli: A Reaction Wheel Based 3D Inverted Pendulum

Mohanarajah Gajamohan, Michael Muehlebach, Tobias Widmer, and Raffaello D'Andrea

***Abstract*— The Cubli is a $15 \times 15 \times 15$ cm cube with reaction wheels mounted on three of its faces. By applying controlled torques to the reaction wheels the Cubli is able to balance on its corner or edge. This paper presents the development of the Cubli. First, the mechatronic design of the Cubli is presented. Then the multi-body system dynamics are derived. The parameters of the nonlinear system are identified using a frequency domain based approach while the Cubli is balancing on its edge with a nominal controller. Finally, the corner balancing using a linear feedback controller is presented along with experimental results.**

I. INTRODUCTION

For slightly more than a century, inverted pendulum systems have been an indispensable part of the controls community [1]. They have been widely used to test, demonstrate and benchmark new control concepts and theories [2]. Algorithms for controlling pendulum systems are an active area of research today [3]–[5].

Compared to other 3D inverted pendulum test-beds [6], [7] the Cubli has two unique features. One is its relatively small footprint, (hence the name Cubli, which is derived from the Swiss German diminutive for "cube"). The other feature, demonstrated in Fig. 2, is the Cubli's ability to jump up from a resting position without any external support, by suddenly braking its reaction wheels rotating at high speeds. The concept of jumping up is covered in [8], while this paper focuses on the balancing aspect.

The remainder of this paper is structured as follows: Sec. II presents a brief overview of the Cubli's mechanical and electronic design. This is followed by the derivations of the system dynamics in III and system identification in Sec. IV. Sec. V covers the state estimation algorithm. Finally, the controller and the experimental results are presented in Sec. VI.

II. MECHATRONIC DESIGN

Fig. 3 shows the CAD model of the Cubli, which consists of an aluminium housing holding three reaction wheels through the motors. Although a light weight housing would result in high recovery angles, it must be strong enough to withstand the impact-based braking during jump-up [8].

With respect to electronics, everything except the power source is mounted in the Cubli. A simplified diagram of the electronics is presented in Fig. 4. The STM32 discovery board (ARM7 Cortex-M4, 168MHz) from STMicroelectronics is used as the Cubli's main controller. Six IMUs (MPU-6050, InvenSense), one on each face of the Cubli, are used for tilt estimation. Each IMU consists of a rate gyro and an accelerometer, and is connected to the main controller through the I2C bus. A 50 W brushless DC motor, EC-45-flat, from Maxon Motor AG is used to drive the reaction wheels. The three brushless DC motors are controlled by three DEC 36/2 modules, digital four quadrant brushless DC motor controllers. The motor controller and main controller communicate over the CANopen protocol.

Finally on the software side, The STM32 port of the FreeRTOS scheduler is used for the multitasking of the estimation and control algorithms and an Eclipse based tool chain is used for development.

The authors are with the Institute for Dynamic Systems and Control, Swiss Federal Institute of Technology Zürich, Switzerland. The contact author is M. Gajamohan, e-mail: gajan@ethz.ch.

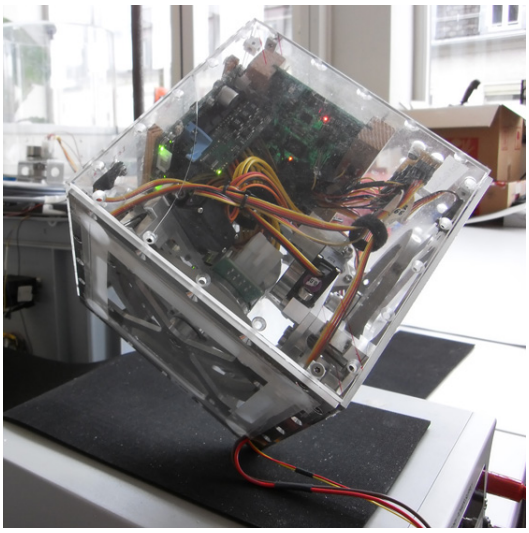

Fig. 1. Cubli balancing on the corner. In the current version, the Cubli (controller) must be started while holding the Cubli near the equilibrium position. Power is provided from an external constant voltage supply.

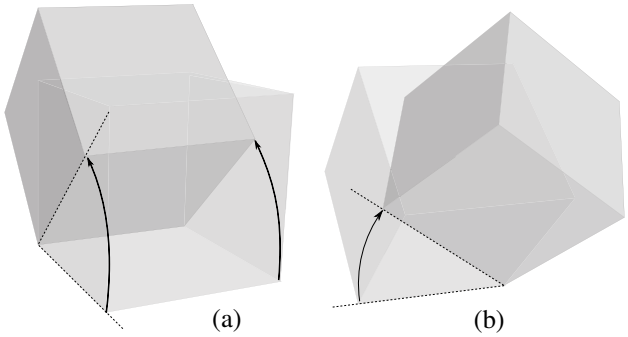

Fig. 2. The Cubli jump-up strategy: (a) Flat to Edge: Initially lying flat on its face, the Cubli jumps up to stand on its edge. (b) Edge to Corner: The Cubli goes from balancing on an edge to balancing on a corner.

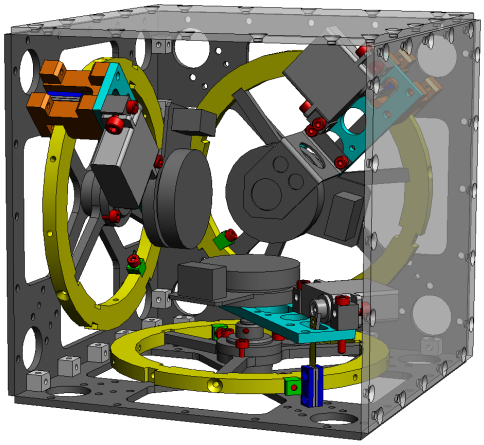

Fig. 3. The CAD drawing of the Cubli with one of the acrylic glass covers removed.

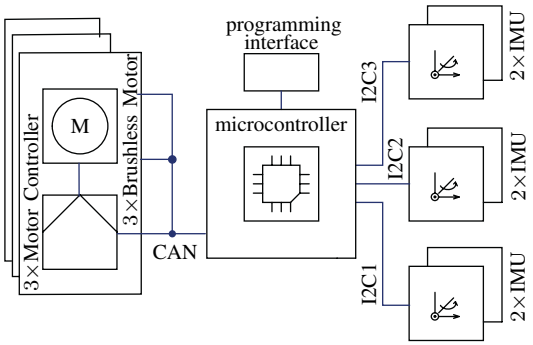

Fig. 4. The Cubli electronics schematic: Six IMUs (rate-gyro and accelerometer) are connected to the ARM7 microcontroller with three I2C buses. The three motor controllers communicate with the microcontroller over the CAN bus.

III. SYSTEM DYNAMICS

In this section the nonlinear dynamics of the Cubli are derived using Kane's equations and the dynamics are linearized around the upright equilibrium position. The linearized dynamics will be used for system identification and corner balancing in the following sections.

With respect to the notations of this paper, let $\mathbb{R}$, $\mathbb{C}$ and $\mathbb{N}$ denote the set of real, complex, and natural numbers. For attitude representations we adopt [9], where ${}^A_B R \in SO(3)$ describes the rotation of frame $\{B\}$ relative to frame $\{A\}$. Note that the column vectors of ${}^A_B R$ are the unit vectors of $\{B\}$ expressed in $\{A\}$. Furthermore, e_i denotes the unit vector with a single non zero element at i and $\tilde{v}_1 \in \mathbb{R}^{3\times 3}$ is the skew symmetric matrix of the vector $v_1 \in \mathbb{R}^3$ where $\tilde{v}_1 v_2 \equiv v_1 \times v_2$, for all $v_2 \in \mathbb{R}^3$. Unless otherwise noted by a proceeding superscript all quantities are represented in the Cubli body fixed frame $\{B\}$.

A. Nonlinear System Dynamics

Consider the Cubli balancing on its corner, as shown in Fig. 5. Let $\omega_{\mathrm{h}} \in \mathbb{R}^3$ denote the angular velocity of the Cubli relative to the inertial frame $\{I\}$ expressed in the Cubli's body fixed frame $\{B\}$, $\omega_{\mathrm{w}i} \in \mathbb{R}$, $i = 1, 2, 3$ denote the angular velocities of the wheels around the rotational axis ${}_B e_i$, and ${}^I_B R \in SO(3)$ denote the attitude of the Cubli relative to the inertial frame $\{I\}$. Note that attitude of the Cubli can also be represented by the zyx-Euler angles $\phi = (\mathrm{yaw}(\alpha),\ \mathrm{pitch}(\beta),\ \mathrm{roll}(\gamma))$. The relationship between the rotation matrix and Euler angle representation is given by

$$ {}^B_I R = e^{\tilde{e}_3 \alpha} e^{\tilde{e}_2 \beta} e^{\tilde{e}_1 \gamma}, \tag{1} $$

where e is the matrix exponential. The nonlinear system dynamics are derived using Kane's equation [10] for multi bodies given by

$$ \delta v^{\mathrm{T}} \sum_{\forall j} \left[J_{P_j}^{\mathrm{T}} \dot{p}_j + J_{R_j}^{\mathrm{T}} \dot{n}_j - J_{P_j}^{\mathrm{T}} F_j^a - J_{R_j}^{\mathrm{T}} T_j^a \right] = 0, \tag{2} $$

for all $\delta v \neq 0$, where

$$ v := (\omega_{\mathrm{h}}, \omega_{\mathrm{w}1}, \omega_{\mathrm{w}2}, \omega_{\mathrm{w}3}) \in \mathbb{R}^6 \tag{3} $$

denotes generalized velocity, j denotes a particular rigid body of the multi-body system, p_j the linear momentum of the rigid body j, n_j the angular momentum, F_j^a the external active force, T_j^a the external active torque, and J_{*j} the Jacobian matrix. Geometrically, Kane's equation can be interpreted as the projection of the Newton-Euler equation on to the configuration manifold's tangent space [11].

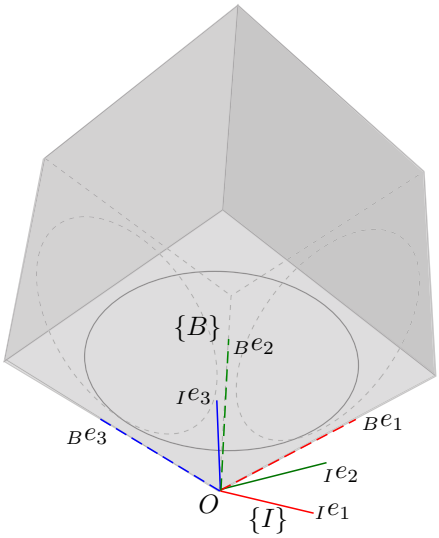

Fig. 5. Cubli balancing on the corner. ${}_B e_*$ and ${}_I e_*$ denote the principle axis of the body fixed frame $\{B\}$ and inertial frame $\{I\}$. The pivot point O is the common origin of coordinate frames $\{I\}$ and $\{B\}$.

Consider the Cubli as a multi-body system consisting of four rigid bodies: The Cubli housing h and three reaction wheels w1, w2, and w3.

First, consider the Cubli housing h and let r_{h} denote the position of the center of mass of the Cubli frame expressed in Cubli body fixed frame $\{B\}$. Now, using

$$ \dot{r}_{\mathrm{h}} = \omega_{\mathrm{h}} \times r_{\mathrm{h}} \quad \text{and} \tag{4} $$

$$ \ddot{r}_{\mathrm{h}} = \dot{\omega}_{\mathrm{h}} \times r_{\mathrm{h}} + \omega_{\mathrm{h}} \times (\omega_{\mathrm{h}} \times r_{\mathrm{h}}) \tag{5} $$

the time derivative of the housing's linear momentum is given by

$$\dot{p}_{\mathrm{h}} = m_{\mathrm{h}} \left(\dot{\omega}_{\mathrm{h}} \times r_{\mathrm{h}} + \omega_{\mathrm{h}} \times (\omega_{\mathrm{h}} \times r_{\mathrm{h}}) \right). \quad (6)$$

Similarly, the time derivative of the housing's angular momentum $n_{\mathrm{h}} := \Theta_{\mathrm{h}} \omega_{\mathrm{h}}$ is given by

$$\dot{n}_{\mathrm{h}} = \Theta_{\mathrm{h}} \dot{\omega}_{\mathrm{h}} - (\Theta_{\mathrm{h}} \omega_{\mathrm{h}}) \times \omega_{\mathrm{h}}, \quad (7)$$

where $\Theta_{\mathrm{h}} \in \mathrm{R}^{3\times 3}$ is the inertia tensor of the Cubli housing h.

Next, consider the i^{th} wheel, $i = 1, 2, 3$, with angular velocity given by $\omega_{\mathrm{w}i} e_i + \omega_{\mathrm{h}}$. The time derivative of the wheel's linear momentum is given by

$$\dot{p}_{\mathrm{w}i} = m_{\mathrm{w}} \left(\dot{\omega}_{\mathrm{h}} \times r_{\mathrm{w}i} + \omega_{\mathrm{h}} \times (\omega_{\mathrm{h}} \times r_{\mathrm{w}i}) \right), \quad (8)$$

where $r_{\mathrm{w}i}$ is the position of wheel center of mass. The angular momentum of the wheel and its time derivative are given by

$$\begin{aligned} n_{\mathrm{w}i} &= \Theta_{\mathrm{w}i} \omega_{\mathrm{h}} + \Theta_{\mathrm{w}i}(i,i) \omega_{\mathrm{w}i} e_i \\ \dot{n}_{\mathrm{w}i} &= \Theta_{\mathrm{w}i} \dot{\omega}_{\mathrm{h}} - (\Theta_{\mathrm{w}i} \omega_{\mathrm{h}}) \times \omega_{\mathrm{h}} \\ &\quad + \Theta_{\mathrm{w}i}(i,i) \dot{\omega}_{\mathrm{w}i} e_i - (\Theta_{\mathrm{w}i}(i,i) \omega_{\mathrm{w}i} e_i) \times \omega_{\mathrm{h}}, \quad (9) \end{aligned}$$

where $\Theta_{\mathrm{w}i} \in \mathbb{R}^{3\times 3}$ is the inertia tensor of the reaction wheel wi.

The Jacobian matrices related to the Cubli housing h are given by

$$J_{P_{\mathrm{h}}} = \frac{\partial}{\partial v} \dot{r}_{\mathrm{h}} \underset{(4)}{=} (-\tilde{r}_{\mathrm{h}}, 0, 0, 0) \in \mathbb{R}^{3\times 6} \quad (10)$$

$$J_{R_{\mathrm{h}}} = \frac{\partial}{\partial v} \dot{\omega}_{\mathrm{h}} = (I, 0, 0, 0) \in \mathbb{R}^{3\times 6} \quad (11)$$

and Jacobian matrices related to the wheels are given by

$$J_{P_{\mathrm{w}i}} = \frac{\partial}{\partial v} \dot{r}_{\mathrm{w}i} = (-\tilde{r}_{\mathrm{w}i}, 0, 0, 0) \in \mathbb{R}^{3\times 6} \quad (12)$$

$$J_{R_{\mathrm{w}i}} = \frac{\partial}{\partial v} \left(\omega_{\mathrm{w}i} e_i + \omega_{\mathrm{h}} \right) = (I, \delta_i) \in \mathbb{R}^{3\times 6}, \quad (13)$$

where $\delta_i \in \mathbb{R}^{3\times 3}$ has all zero elements except for the i^{th} diagonal element, which is one.

The active torque on the Cubli housing and the wheels are given by

$$\begin{aligned} -T_{\mathrm{h}} &= (T_{\mathrm{w}1}, T_{\mathrm{w}2}, T_{\mathrm{w}3}) \\ &= K_m u - C_{\mathrm{w}}(\omega_{\mathrm{w}1}, \omega_{\mathrm{w}2}, \omega_{\mathrm{w}3}), \quad (14) \end{aligned}$$

where K_m is the motor constant, $u := (u_1, u_2, u_3) \in \mathbb{R}^3$ is the current input of each motor driving the wheels, and C_{w} is the damping constant. Finally, gravity g leads to an active force on all bodies. Note that g is expressed in the body fixed frame $\{B\}$ and given by

$$g(\phi) = g_0(s(\beta), -s(\gamma)c(\beta), -c(\gamma)c(\beta)), \quad (15)$$

where $g_0 = 9.81 \ \mathrm{m \cdot s^{-2}}$.

Now, inserting (6) to (14) into (2) yields the following equations of motion

$$\begin{aligned} \hat{\Theta} \dot{\omega}_{\mathrm{h}} &= \Theta \omega_{\mathrm{h}} \times \omega_{\mathrm{h}} + Mg + \Theta_{\mathrm{w}} \omega_{\mathrm{w}} \times \omega_{\mathrm{h}} \\ &\quad - (K_m u - C_{\mathrm{w}} \omega_{\mathrm{w}}) \\ \Theta_{\mathrm{w}} \dot{\omega}_{\mathrm{w}} &= K_m u - C_{\mathrm{w}} \omega_{\mathrm{w}} - \Theta_{\mathrm{w}} \dot{\omega}_{\mathrm{h}}, \ i = 1, 2, 3, \quad (16) \end{aligned}$$

where

$$\begin{aligned} M &= m_{\mathrm{h}} \tilde{r}_{\mathrm{h}} + \sum_{i=1}^{3} m_{\mathrm{w}i} \tilde{r}_{\mathrm{w}i} \\ \Theta &= \Theta_{\mathrm{h}} - m_{\mathrm{h}} \tilde{r}_{\mathrm{h}}^2 + \sum_{i=1}^{3} \left[\Theta_{\mathrm{w}i} - m_{\mathrm{w}} \tilde{r}_{\mathrm{w}i}^2 \right], \\ \Theta_{\mathrm{w}} &= \mathrm{diag}(\Theta_{\mathrm{w}1}(1,1), \Theta_{\mathrm{w}2}(2,2), \Theta_{\mathrm{w}3}(3,3)), \\ \hat{\Theta} &= \Theta - \Theta_{\mathrm{w}}. \end{aligned}$$

Finally, the kinematic equation of the Cubli is given by

$$\omega_{\mathrm{h}} = \begin{pmatrix} -s(\beta) & 0 & 1 \\ s(\gamma)c(\beta) & c(\gamma) & 0 \\ c(\gamma)c(\beta) & -s(\gamma) & 0 \end{pmatrix} \begin{pmatrix} \dot{\alpha} \\ \dot{\beta} \\ \dot{\gamma} \end{pmatrix}. \quad (17)$$

B. Linearized Dynamics

This subsection derives the linearized dynamics of Cubli around the upright equilibrium position. The models derived here will be used for the system identification in Sec. IV and corner balancing in Sec. VI.

The Cubli's equilibrium attitude ϕ_0 is the solution of

$$Mg(\phi) = 0, \quad (18)$$

and all angular velocities at equilibrium are zero, $\omega_{\mathrm{h}0} = 0$, $\omega_{\mathrm{w}i} = 0$, $i = 1, 2, 3$.

Inverting (17) and inserting the equilibrium attitude ϕ_0 yields the first part of the linearized system equation:

$$\begin{pmatrix} \dot{\hat{\alpha}} \\ \dot{\hat{\beta}} \\ \dot{\hat{\gamma}} \end{pmatrix} = \begin{pmatrix} 0 & \frac{s(\gamma_0)}{c(\beta_0)} & \frac{c(\gamma_0)}{c(\beta_0)} \\ 0 & c(\gamma_0) & -s(\gamma_0) \\ 1 & \frac{s(\gamma_0)s(\beta_0)}{c(\beta_0)} & \frac{c(\gamma_0)s(\beta_0)}{c(\beta_0)} \end{pmatrix} \hat{\omega}_{\mathrm{h}} := F \hat{\omega}_{\mathrm{h}}, \quad (19)$$

where $\hat{}$ denotes the deviations from their equilibrium values. Since the terms $\Theta \omega_{\mathrm{h}} \times \omega_{\mathrm{h}}$ and $\Theta_{\mathrm{w}} \omega_{\mathrm{w}} \times \omega_{\mathrm{h}}$ vanish in the linearization around $\omega_{\mathrm{h}0}$, leading to

$$\begin{aligned} \dot{\hat{\omega}}_{\mathrm{h}} &= \hat{\Theta}^{-1} \left[M \left. \frac{\partial g(\phi)}{\partial \phi} \right|_{\phi_0} \hat{\phi} + C_{\mathrm{w}} \hat{\omega}_{\mathrm{w}} - K_M \hat{u} \right] \\ \dot{\hat{\omega}}_{\mathrm{w}} &= -\hat{\Theta}^{-1} M \left. \frac{\partial g(\phi)}{\partial \phi} \right|_{\phi_0} \hat{\phi} \\ &\quad - (\hat{\Theta}^{-1} + \Theta_{\mathrm{w}}{}^{-1}) C_{\mathrm{w}} \hat{\omega}_{\mathrm{w}} + (\hat{\Theta}^{-1} + \Theta_{\mathrm{w}}^{-1}) K_M \hat{u}, \quad (20) \end{aligned}$$

where

$$\left. \frac{\partial g(\phi)}{\partial \phi} \right|_{\phi_0} = \begin{pmatrix} 0 & c(\beta_0) & 0 \\ 0 & s(\beta_0)s(\gamma_0) & -c(\beta_0)c(\gamma_0) \\ 0 & s(\beta_0)c(\gamma_0) & c(\beta_0)s(\gamma_0) \end{pmatrix}.$$

Now, putting (19) and (20) together results in

$$\begin{pmatrix} \dot{\hat{\phi}} \\ \dot{\hat{\omega}}_{\mathrm{h}} \\ \dot{\hat{\omega}}_{\mathrm{w}} \end{pmatrix} = A \begin{pmatrix} \hat{\phi} \\ \hat{\omega}_{\mathrm{h}} \\ \hat{\omega}_{\mathrm{w}} \end{pmatrix} + \begin{pmatrix} 0_{3\times 3} \\ -\hat{\Theta}^{-1} K_M \\ (\hat{\Theta}^{-1} + \Theta_{\mathrm{w}}^{-1}) K_M \end{pmatrix} \hat{u}, \quad (21)$$

where

$$A = \begin{pmatrix} 0_{3\times3} & F & 0_{3\times3} \\ \hat{\Theta}^{-1}M\left.\frac{\partial g(\phi)}{\partial \phi}\right|_{\phi_0} & 0_{3\times3} & C_{\mathrm{w}}\hat{\Theta}^{-1} \\ -\hat{\Theta}^{-1}M\left.\frac{\partial g(\phi)}{\partial \phi}\right|_{\phi_0} & 0_{3\times3} & -C_{\mathrm{w}}(\hat{\Theta}^{-1}+\Theta_{\mathrm{w}}^{-1}) \end{pmatrix}.$$

IV. SYSTEM IDENTIFICATION

This section describes an offline frequency domain based approach for estimating the parameters

$$\eta := (K_m, C_{\mathrm{w}}, \Theta, \Theta_{\mathrm{w}}, r_{\mathrm{h}}) \tag{22}$$

of (16) that can not be directly measured. As the first step of parameter estimation, the Cubli is made to balance on its edge, as shown in Fig. 6, using a linear feedback controller K derived from nominal model parameters (See Fig. 7). The equations of motion can be obtained by setting $\omega_{\mathrm{h}} = (\dot{\theta}_{\mathrm{h}}, 0, 0)$, $\omega_{\mathrm{w}} = (\dot{\theta}_{\mathrm{w}}, 0, 0)$ in (16). Hence, inserting this into equation (21) yields the linearized dynamics around the upright position, when the Cubli is balancing on its edge. Taking $x_{e_1} = (\hat{\gamma} - \gamma_0, \dot{\hat{\theta}}_{\mathrm{h}}, \dot{\hat{\theta}}_{\mathrm{w}})$ results in

$$\dot{x}_{e_1}(t) = A_{e_1}(\eta)x_{e_1}(t) + B_{e_1}(\eta)u_1(t). \tag{23}$$

Now, let

$$G(s,\eta) := (I - sA_{e_1}(\eta))^{-1}B_{e_1} =: \begin{pmatrix} G_1(s,\eta) \\ G_2(s,\eta) \\ G_3(s,\eta) \end{pmatrix} \tag{24}$$

denote the transfer function of (23) where G_1, G_2 and G_3 are the transfer functions from input current u_1 to θ_{h}, $\dot{\hat{\theta}}_{\mathrm{h}}$ and $\dot{\hat{\theta}}_{\mathrm{w}}$ respectively.

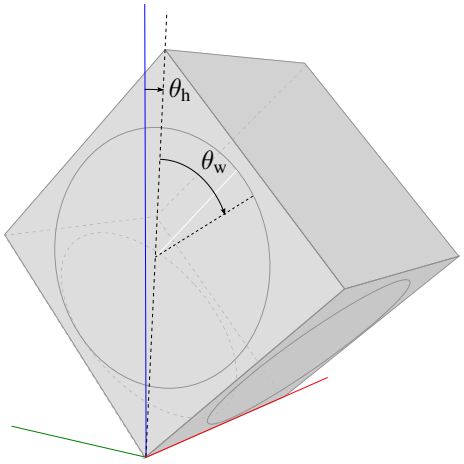

Fig. 6. Cubli balancing on an edge. θ_{h} denotes the tilt angle of the Cubli housing and θ_{w} denotes rotational displacement of the reaction wheel.

While balancing on its edge, the Cubli was excited by the following random phase multisine signal,

$$r(t) = \sum_{k=1}^{\infty} A_k \sin(2\pi f_s k t + \psi_k), \quad A_k \in \mathbb{R}^+, \tag{25}$$

where the sampling frequency $f_s = 50$ Hz and ψ_k is randomly distributed in $[0, 2\pi)$. Note that, due to its periodicity, the above random phase multisine signal prevents spectral leakage. Also, due to its randomness, the impact of the nonlinearities can be estimated by comparing averages over consecutive periods and different realizations [12]. A realization is defined by a set of $\{A_k, \psi_k\}$, $k \in \mathbb{N}$. In our case only a finite number of non zero A_ks were used. The signal that corresponds to the p^{th} period of a certain realization r is denoted by the superscript $[r,p]$.

Now, consider the frequency response under the excitation signal given in (25). Let $y(t) \in \mathbb{R}$ denote the output of the Cubli disturbed with Gaussian white noise, $r(t)$ the reference signal, $u(t)$ the resulting input, and $\hat{g}(t) \in \mathbb{R}^3$ the impulse response of the underlying linear system. Next, let $Y(\omega)$, $\hat{G}(\omega)$, $U(\omega)$, $R(\omega)$ denote the Fourier transforms of $y(t)$, $\hat{g}(t)$, $u(t)$, and $r(t)$ respectively.

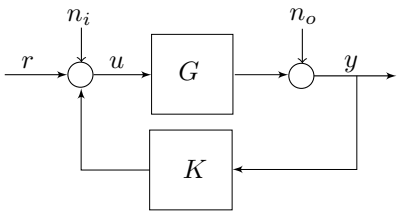

Fig. 7. The block diagram of the system identification procedure: The edge balancing system G is controlled by a nominal linear feedback controller K and is excited by the random phase multisine signal r. n_i and n_o denote the Gaussian white noise on the input and output of the system.

Assuming Gaussian white noise disturbances on the input and output signals gives the following maximum likelihood estimate for the frequency response function (FRF):

$$\hat{G}(\omega) = \frac{Y_R(\omega)}{U_R(\omega)} = \frac{\frac{1}{R}\sum_{r=1}^{R} Y(\omega)^{[r]}}{\frac{1}{R}\sum_{r=1}^{R} U(\omega)^{[r]}} \tag{26}$$

where

$$Y(\omega)^{[r]} = \frac{1}{P}\sum_{p=1}^{P} Y(\omega)^{[r,p]} e^{-j\psi_\omega}, \quad \text{and}$$

$$U(\omega)^{[r]} = \frac{1}{P}\sum_{p=1}^{P} U(\omega)^{[r,p]} e^{-j\psi_\omega}.$$

Note that in order to average over different realizations, the phase of the measured quantities, $U(\omega)^{[r,p]}$ and $Y(\omega)^{[r,p]}$, was adjusted with respect to the reference signal.

Since the underlying system is nonlinear, different input realizations will lead to different FRF estimates. Hence by comparing the noise levels of the FRF estimates over different realisations, the impact of nonlinearities can be evaluated. The noise impact on one realization is approximated by

$$\hat{\sigma}^2_{XZ^{[r]}}(\omega) = \frac{1}{P(P-1)}\sum_{p=1}^{P}\Big[(X(\omega)^{[r,p]} - X(\omega)^{[r]}) \cdot (Z(\omega)^{[r,p]} - Z(\omega)^{[r]})^*\Big] \tag{27}$$

where X and Z can be Y or U and * denotes the complex conjugate. This in turn gives the noise impact on FRF estimate

$$\hat{\sigma}^2_{XZ,n}(\omega) = \frac{1}{R^2}\sum_{r=1}^{R}\hat{\sigma}_{XZ^{[r]}}(\omega). \tag{28}$$

Now, with sample (co)variances given by

$$\begin{aligned}\hat{\sigma}^2_{X_RZ_R}(\omega) &= \frac{1}{R(R-1)}\sum_{r=1}^{R}\Big[(X(\omega)^{[r]} - X_R(\omega)) \\ &\quad \cdot(Z(\omega)^{[r]} - Z_R(\omega))^*\Big] \end{aligned}\tag{29}$$

the variance on the FRF containing the measurement noise and nonlinear effects is calculated as

$$\begin{aligned}\hat{\sigma}^2_{GG}(\omega) &= \frac{1}{|U_R(\omega)|^2}\Big(\hat{\sigma}^2_{Y_RY_R}(\omega) + \hat{G}(\omega)\hat{\sigma}^2_{U_RU_R}(\omega)\hat{G}^*(\omega) \\ &\quad -\hat{\sigma}^2_{Y_RU_R}(\omega)\hat{G}^*(\omega) - \hat{G}(\omega)\hat{\sigma}^2_{U_RY_R}(\omega)\Big)\end{aligned}\tag{30}$$

The experiments were repeated on all three edges of the actuated face. While the Cubli was balancing, it was excited by a flat (equal amplitude at each frequency component) random phase multisine signal, with a frequency grid of 0.1 Hz ranging from 0.1 Hz to 5.0 Hz. Responses of four different realisations $(R = 4)$ for seven consecutive periods $(P = 7)$ were recorded to evaluate $\hat{G}$ together with its total variance $\hat{\sigma}_{GG}$ and noise variance $\hat{\sigma}_{GG,n}$.

Fig. 8 shows the frequency responses related to the transfer function G_2 in (24), when balancing on the edge that lies along ${}_Be_1$, which is the first principle axis of the body fixed coordinate frame $\{B\}$ (see Fig. 5). $\hat{G}$ is shown in green along with $\hat{\sigma}_{G_2G_2}$ in red and $\hat{\sigma}_{G_2G_2,n}$ in light blue. Note that the additional variance due to nonlinearities is clearly visible (5 dB) and the signal to noise ratio is more than 15 dB. In the next step, the parametric estimate of $G(s,\eta)$ in (24) is found by minimizing the maximum likelihood cost function given by

$$\begin{aligned}V_{ML} &= \sum_{\forall\omega:A_\omega\neq 0} e^*(\omega)\left(\hat{\sigma}^2_{GG}(\omega)|U_R(\omega)|^2\right)^{-1}e(\omega) \\ e(\omega) &:= Y_R(\omega) - G(\omega,\eta)U_R(\omega).\end{aligned}$$

The frequency response of the transfer function G_2 derived from the above minimization is shown in Fig. 8 in blue, along with the fitting error in purple. The uncorrelated fitting error indicates a good approximation of the frequency response measurement by the parametric model.

Note that the system identification procedure presented in this section assumes that the inertia tensor of the full Cubli has no cross couplings. To identify the cross coupling terms the above procedure has to be repeated when the Cubli is balancing on its corner.

V. STATE ESTIMATION

The angular velocity ω_{h} estimates are calculated by averaging the six rate-gyro measurements. The wheel velocity $\omega_{\mathrm{w}i}$, $i = 1,2,3$, estimates come directly from the motor controller. For tilt estimation, the multiple accelerometer based algorithm presented in [7] was implemented.

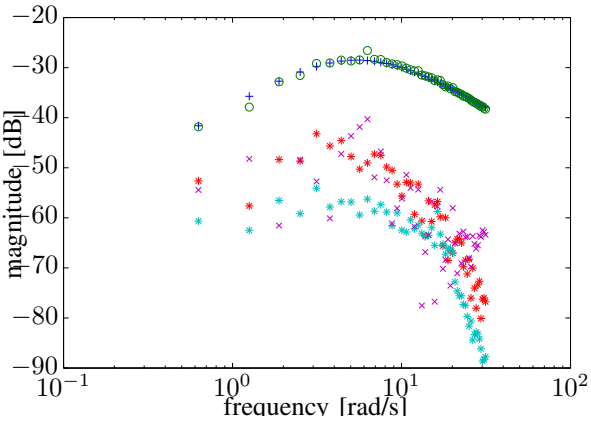

Fig. 8. Frequency responses related to the transfer function G_2 in (24): Magnitude of the measured frequency response function $\hat{G}_2$ is shown is green. The standard deviation $\hat{\sigma}_{G_2G_2}$ is shown in red. The noise standard deviation $\hat{\sigma}_{G_2G_2,n}$ is shown in light blue. The blue markers show the response of the estimated G_2 by minimizing (31). Finally, the uncorrelated purple markers show the absolute error between the parameter model and and the experimental response.

For the tilt estimation the Cubli uses six accelerometers, each attached to one of the Cubli's faces and their positions in the body fixed frame $\{B\}$ is known and denoted by p_i, $i = 1,\ldots,6$.

A noise-free accelerometer measurement ${}^{\hat{A}_i}m_i$ of accelerometer i is given by

$${}^{\hat{A}_i}m_1 = {}^{\hat{A}_i}_{B}R\ {}^{B}_{I}R\ ({}^{I}_{B}\ddot{R}\ {}^{B}p_i + {}^{I}g), \tag{31}$$

where $\{\hat{A}_i\}$ denotes the local frame of the i^{th} sensor, ${}^{I}g$ is the gravity vector expressed in the inertial frame $\{I\}$, and ${}^{I}_{B}\ddot{R}$ is the second derivative of ${}^{I}_{B}R$ satisfying

$${}^{I}\ddot{p}_i = {}^{I}_{B}\ddot{R}\,{}^{B}p_i. \tag{32}$$

Now, changing the reference frames to the body fixed frame $\{B\}$ in (31) by multiplying both sides by ${}^{B}_{\hat{A}_i}R$ gives

$${}^{B}m_i = \tilde{R}\ {}^{B}p_i + {}^{B}g, \tag{33}$$

where $\tilde{R} = {}^{B}_{I}R\ {}^{I}_{B}\ddot{R}$.

Using all accelerometer measurements (33) can be expressed as a matrix equation of the following form

$$M = QP, \tag{34}$$

where

$$\begin{aligned}M &:= \begin{bmatrix} {}^{B}m_1 & {}^{B}m_2 & \cdots & {}^{B}m_6 \end{bmatrix} \in \mathbb{R}^{3\times 6}, \\ Q &:= \begin{bmatrix} {}^{B}g & \tilde{R} \end{bmatrix} \in \mathbb{R}^{3\times 4}, \\ P &:= \begin{bmatrix} 1 & 1 & \cdots & 1 \\ p_1 & p_2 & \cdots & p_6 \end{bmatrix} \in \mathbb{R}^{4\times 6}.\end{aligned}$$

The optimal estimate of Q under noisy measurements, while Q is restricted to linear combinations of measurements M is given by [7]

$$\hat{Q} = M\hat{X}, \quad \hat{X} := P^{\mathrm{T}}(PP^{\mathrm{T}})^{-1}. \tag{35}$$

Finally, this gives the gravity vector estimate

$$^{B}\hat{g} = M\hat{X}(:,1) \tag{36}$$

as a linear combination of measurements M. Note that, since $\hat{X}$ in (36) depends only the sensor positions, it can be calculated offline to make the estimation process run relatively fast. Although, $^{B}\hat{g}$ gives the tilt angles β, γ, $^{B}\hat{g}$ was fused with the rate-gyro measurements to reduce the noise levels. See [7] for more details.

In contrast to many standard methods for state estimation, the above tilt estimator does not require a model of the systems dynamics; the only required information is the location of the sensors on the rigid body. Since no near-equilibrium assumption is made and the nonlinear estimator yields a global tilt estimate, this method will function both for balancing and during the jump-up motion of the Cubli (state information during the jump up phase is needed in order to trigger the switch to balancing mode). The latter would be cumbersome to obtain with standard linear state estimation methods.

VI. CONTROL

This section presents the design procedure of the corner balancing controller, based on the linearized equations of motion given in (21). In the first step, it is shown that the dynamics of the yaw angle α, which is an unobservable state, is decoupled from the rest. Then, the uncontrollable parts of the remaining dynamics are identified. Finally, the uncontrollable states are eliminated through an appropriate coordinate transformation and an LQR based controller is implemented.

Since g is independent of the yaw angle α, the first column of $\frac{\partial g(\phi)}{\partial \phi}\Big|_{\phi_0}$ is $0_{3\times 1}$, which gives $A(:,1) = 0_{9\times 1}$. As a result, the sytem matrix A (21) can be split as

$$\begin{aligned} A &= \left(\begin{array}{c|cc} 0 & 0_{1\times 2} & F(1,:) \;\; 0_{1\times 3} \\ \hline 0_{8\times 1} & \begin{matrix} 0_{2\times 2} \\ \cdot \\ \cdot \end{matrix} & \begin{matrix} F(2:3,:) \\ 0_{3\times 3} \\ 0_{3\times 3} \end{matrix} & \begin{matrix} 0_{2\times 3} \\ \cdot \\ \cdot \end{matrix} \end{array}\right) \\ &=: \left(\begin{array}{c|c} 0 & A_\alpha \\ \hline 0_{8\times 1} & \hat{A} \end{array}\right). \end{aligned}$$

This shows that the dynamics of the unobservable yaw angle α is an open integrator given by

$$\dot{\alpha} = F(1,:)\omega_{\mathrm{b}}. \tag{37}$$

Now, consider the remaining dynamics given by $\hat{A} \in \mathbb{R}^{8\times 8}$. The observation

$$F\ {}^{B}_{I}e_3 = e_1 \tag{38}$$

implies $(0_{2\times 1}, {}^{B}_{I}e_3, 0_{3\times 1})$ is an eigenvector of $\hat{A}$ with eigenvalue 0, giving an uncontrollable direction of $\hat{A}$. Note that ${}^{B}_{I}e_3$ is the third principle axis of the inertial frame expressed in the body fixed frame $\{B\}$ coordinates. From the mechanics perspective, this fact can be interpreted as the conservation of angular momentum along ${}_{I}e_3$ axis (see Fig. 5). Since the Popov-Belevitch-Hautus (PBH) test for $s = 0$ gives $\mathrm{Rank}[sI - \hat{A}, \hat{B}] < 8$, it can be concluded that the corresponding eigenvector is not controllable.

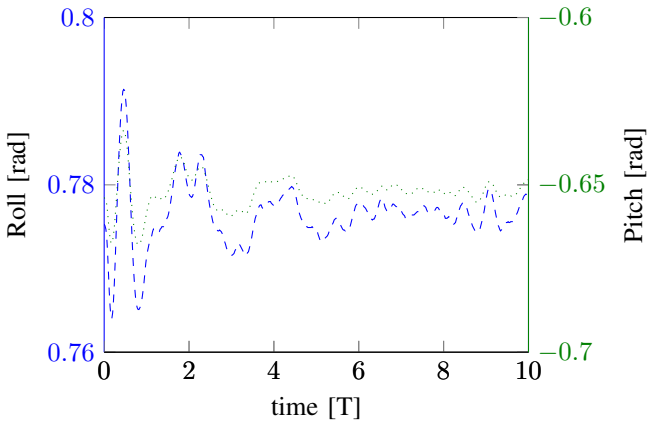

Fig. 9. Time traces of the Cubli's roll(γ) and pitch(β) during a corner balancing experiment. The non zero converging values correspond to the constant bias in attitude measurements.

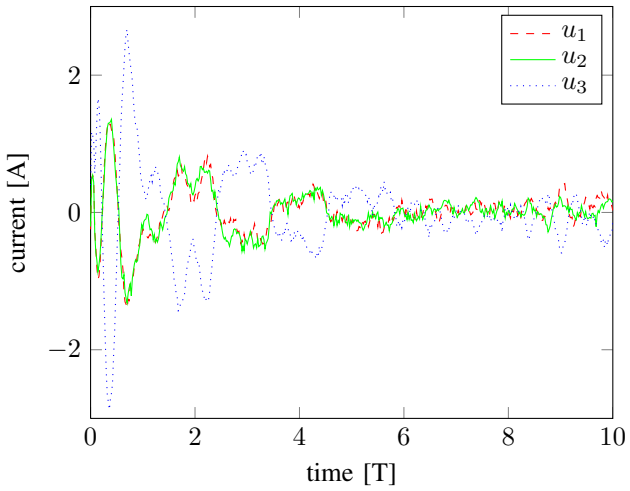

Fig. 10. Time traces of the input current $\{u_1, u_2, u_3\}$ of each motor during a corner balancing experiment.

After eliminating the uncontrollable states by a cannonical coordinate transformation, a Linear Quadratic Regulator (LQR) feedback controller was implemented. Figs. 9,10,11, and 12 show the results of a corner balancing experiment run with an integrator as in [8] to eliminate the constant bias in the attitude measurements.

Furthermore, an additional identification of the parameters of the Cubli, while balancing on its corner would certainly help to get a more accurate model and reduce the oscillations while balancing. Note that the model that is derived from Sec. IV assumes an inertia tensor with no cross couplings. Finally, an accurate model would also lay the foundation for more sophisticated controller designs, e.g. nonlinear controllers.

VII. CONCLUSIONS

This paper tracked the development of the Cubli: a 3D inverted pendulum with a relatively small footprint. First,

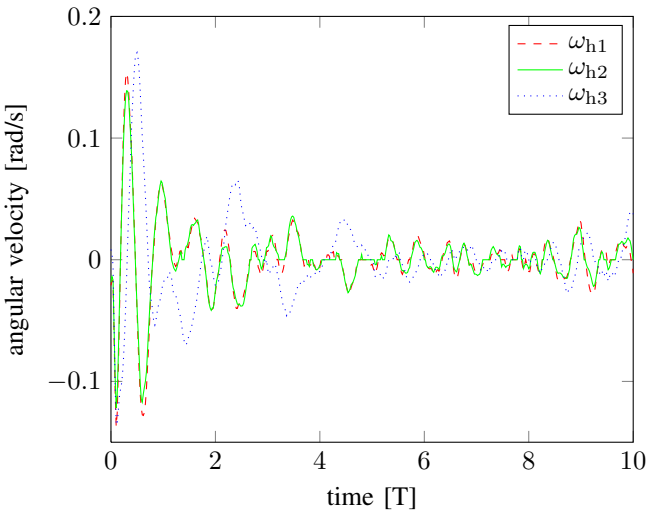

Fig. 11. Time traces of the Cubli's angular velocity ω_h during a corner balancing experiment.

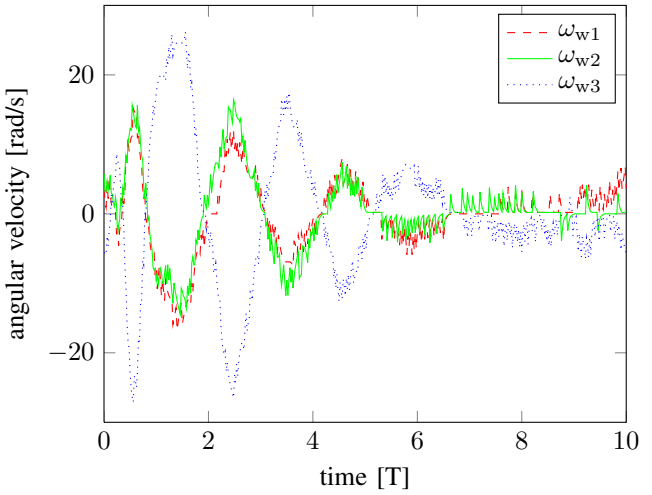

Fig. 12. Time traces of the reaction wheel velocities $\{\omega_{w1}, \omega_{w2}, \omega_{w3}\}$ during a corner balancing experiment.

the mechatronic design was presented, along with a brief reasoning on the design choices. Then the multi body system dynamics were derived using Kane's equation. To estimate the system parameters, a frequency domain based approach, which does not rely on any external apparatus or measurements, was presented. Next the implementation of the accelerometer based global tilt estimator was described. Finally, the corner balancing controller was presented along with experimental results.

ACKNOWLEDGEMENTS

The authors would like to express their gratitude towards Igor Thommen, Marc-Andre Corzillius, and Hans Ulrich Honegger for their significant contribution to the mechanical and electronic design of the Cubli.

REFERENCES

[1] A. Stephenson, "On a new type of dynamical stability," *Proceedings: Manchester Literary and Philosophical Society*, vol. 52, pp. pp. 1–10, 1908.

[2] P. Reist and R. Tedrake, "Simulation-based LQR-trees with input and state constraints," in *Robotics and Automation (ICRA), 2010 IEEE International Conference on*, may 2010, pp. 5504 –5510.

[3] D. Alonso, E. Paolini, and J. Moiola, "Controlling an inverted pendulum with bounded controls," in *Dynamics, Bifurcations, and Control*, ser. Lecture Notes in Control and Information Sciences. Springer Berlin / Heidelberg, 2002, vol. 273, pp. 3–16.

[4] M. V. Bartuccelli, G. Gentile, and K. V. Georgiou, "On the stability of the upside-down pendulum with damping," *Proceedings: Mathematical, Physical and Engineering Sciences*, vol. 458, no. 2018, pp. pp. 255–269, 2002.

[5] J. Meyer, N. Delson, and R. de Callafon, "Design, modeling and stabilization of a moment exchange based inverted pendulum," in *15h IFAC Symposium on System Identification, Saint-Malo, France*, 2009, pp. 462 – 467.

[6] D. Bernstein, N. McClamroch, and A. Bloch, "Development of air spindle and triaxial air bearing testbeds for spacecraft dynamics and control experiments," in *American Control Conference, 2001. Proceedings of the 2001*, vol. 5, 2001, pp. 3967 –3972 vol.5.

[7] S. Trimpe and R. D'Andrea, "Accelerometer-based tilt estimation of a rigid body with only rotational degrees of freedom," in *Robotics and Automation (ICRA), 2010 IEEE International Conference on*, May 2010, pp. 2630 –2636.

[8] M. Gajamohan, M. Merz, I. Thommen, and R. DAndrea, "The cubli: A cube that can jump up and balance," in *Intelligent Robots and Systems (IROS), 2012 IEEE/RSJ International Conference on*, October 2012, pp. 3722–3727.

[9] J. J. Craig, *Introduction to Robotics: Mechanics and Control*, 2nd ed. Boston, MA, USA: Addison-Wesley Longman Publishing Co., Inc., 1989.

[10] T. R. Kane and D. A. Levinson, *Dynamics, Theory and Applications*. McGraw Hill, 1985.

[11] M. Lesser, "A geometrical interpretation of Kane's equations," *Proceedings: Mathematical and Physical Sciences*, vol. 436, no. 1896, pp. pp. 69–87, 1992. [Online]. Available: http://www.jstor.org/stable/52020

[12] R. Pintelon, J. Schoukens, and J. Wiley. (2001) System identification a frequency domain approach. [Online]. Available: http://ieeexplore.ieee.org/xpl/bkabstractplus.jsp?bkn=5237512